Trajectory of an optical vortex in atmospheric turbulence

A. Dipankar,* R. Marchiano, and P. Sagaut
Institut Jean le Rond d'Alembert, UMR CNRS 7190, Université Pierre et Marie Curie-Paris 6, 4 Place Jussieu, Case 162, F-75252 Paris Cedex 5, France

(Received 6 May 2009; revised manuscript received 7 July 2009; published 28 October 2009)

Trajectory of an optical vortex has been identified for its propagation in atmospheric turbulence using numerical simulations. An analytical expression has been found, relating the radial departure of the vortex in plane perpendicular to the direction of propagation, to the refractive index structure function parameter and the inner scale of turbulence. The angular orientation of the vortex in the same transverse plane is found to be related to the anisotropy of the medium. The obtained results provide an alternative way to find turbulent parameters with the help of optical vortices.

DOI: 10.1103/PhysRevE.80.046609 PACS number(s): 42.68.Bz

I. INTRODUCTION

Propagation study of optical vortices [1] has become a growing area of research because of its possible use as information carriers [2] or optical tweezers and spanners [3]. These vortices are of particular interest because they carry orbital angular momentum [4], which can be transmitted to microscopic particles upon collision [5]. It has been noted in early works [2,6] that the presence of an optical vortex may help the carrier light beam to propagate through larger distances, in turbulent medium, as compared to the carrier beams itself. Some theoretical studies have also suggested that they have the ability to reconstruct around certain obstacles [7,8].

In recent years, with the application of laser beams in atmosphere and with the advancement of fast computers, the propagation studies of laser beams in turbulent atmosphere has become very popular [9–14]. However, these studies cited above are mainly restricted to the beams without any phase singularity. Studies dealing with the propagation characteristics of the phase singularity in turbulent medium is very limited and can be found in [2,15–17] and the references therein. In [15] the author demonstrated that the topological charge of a vortex beam is a robust quantity that could be used as an information carrier. An approximate expression of a Bessel-Gaussian beam was proposed in [16] and it was found that the phase singularity rapidly fades away during propagation in turbulent atmosphere. Similar observation was made by the authors in [17] and it was concluded that an optical vortex formed with higher topological charge may propagate over a much longer distance in a moderately or weakly turbulent atmosphere.

It is important to note that all the previous works, dealing with propagation of phase singularities in atmospheric medium, were performed with the assumption that Kolmogorov power law is valid at all the scales of turbulence. It is well known that this law is not valid for both the large (energy carrying input range) and small scales (dissipation range) of turbulence. An ideal spectrum, identifying these important ranges of turbulence, is shown in Fig. 1 for reference. Effect of these scales, on propagation of optical waves without any phase singularities have been already studied by many authors, for example in [9,10]. These studies clearly show that in order to correctly capture the effect of atmospheric turbulence, all the scales of turbulence has to be correctly modeled. This has been achieved in the current research by using the modified von Karman spectra of [18], details of which is provided in the following section. However, it is important to mention at this point that for some of the simulations performed in the text, the chosen turbulent parameters do not conform to the actual (expected) behavior of the atmospheric turbulence. And, the use of such parameters do not affect the generality of the obtained results in any way.

There are some previous works in which the trajectory of an optical vortex has been studied for free-space propagation. For example [19], has formulated rules that constrain the relationships between optical vortex trajectories on a given manifold. His study revealed that many possible trajectories can be eliminated based on simple sign rules. Later in [20], the same author studied relationships that exist between vortex trajectory and their associated stationary point trajectories. They found that the trajectories of these two different types of critical points, one is the vortex and another is simply the intensity null, join together at a junction to form a bundle kind of structure. They also concluded that similar such geometries are present in realistic Gaussian laser also. In an experimental work [21], the authors studied the trajectories of both canonical and noncanonical vortices, also in free space. However, there is no published result, discussing the same for propagation in a turbulent medium. This is the main motive of the present work—to identify the trajectory of an optical vortex in a turbulent medium using numerical simulations.

The trajectory has been identified by following the radial departure (δr) of the initial (primary) vortex from its initial location, and its preferred angular orientation (θ) in a plane perpendicular to the direction of propagation. Laguerre-Gaussian (LG) beam [15] is used to describe a field containing optical vortex of charge +1 and radial order 0. A vortex, by definition, is identified as the point where both real and imaginary part of the wave field are simultaneously equal to zero. Interesting point about an optical vortex is that its zero intensity is due to a destructive interference at its center, which results in a sudden dip (to zero) in the intensity profile

*dipankar.anurag@gmail.com

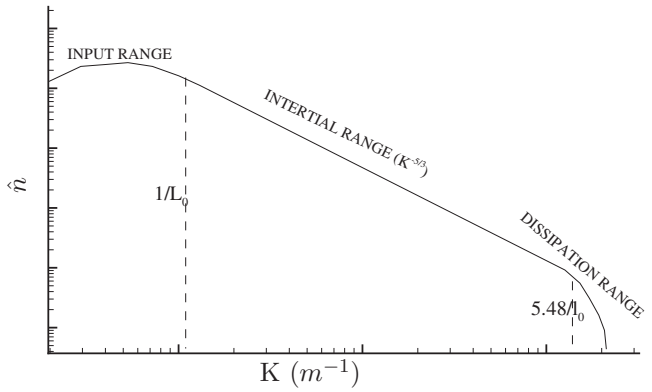

FIG. 1. Schematic of three-dimensional spectrum of the refractive index fluctuations. All important length scales are indicated in the figure for reference.

of the beam, only at the location of the vortex. The immediate neighborhood of the vortex shows the high value in intensity. This implies, that tracking simply an intensity *null* will not ensure the path of a vortex. The null point should have high-intensity values in its neighborhood. This is also clear from the results in [20].

Because of the discrete nature of the computational grid, it is not a trivial task to identify the point of intersection of the real and imaginary zero lines with great accuracy. The only available techniques, that we are aware of, are those given in [22,23]. In [22], the authors suggested a technique based on the Shack-Hartmann wave-front sensor. In [23] the authors have used a technique based on the decomposition of an arbitrary wave field into LG modes. Although, both these techniques are generic in nature and can be used for an arbitrary shape of the wave field, their implementation cost is very high. In order to reduce this cost and thereby increase the simulation speed, we propose a simpler technique based on the contour tracing algorithm used in many plotting softwares.

The originality of the presented work can be categorized as:

(i) Tracking the trajectory of an optical vortex in a realistic atmospheric turbulence. To our knowledge, this has been never tried before.

(ii) Realistic atmospheric turbulence has been obtained using the modified von Karman spectrum for refractive index fluctuations, which includes the effect of both large and small scale fluctuations. Such detailed representation of atmospheric turbulence is unique in the propagation study of optical vortices.

(iii) The obtained results are simple analytic expressions relating the radial departure of the vortex to the turbulent parameters such as refractive index structure function parameter (C_n^2), the inner scale (l_0), and the outer scale (L_0) of the turbulent medium. This finding is unique in the research of singular optics. These expressions also provide the first step to study the atmospheric turbulence with the help of optical vortices.

(iv) The present work lies in identifying the qualitative relationship between the angular orientation of the vortex and the anisotropy of the turbulent medium.

It is important to mention at this point that trajectory has been obtained for a fixed wavelength and width of the initial beam. No attempt has been made to relate the trajectory with these quantities. Scope of the present work lies in establishing a relationship between the vortex trajectory and the various turbulent parameters for a given optical beam.

In the following section, key features of the numerical simulation are briefly given along with the description of the algorithm used to capture the location of the optical vortices. Results on vortex trajectory are presented in Sec. III, in which the relationship of δr with various turbulent parameters and the effect of the medium anisotropy on the vortex trajectory is discussed. Comparison of the radial departure (or drift) of the vortex with that of the centroid of its parent (Gaussian) beam is done in Sec. IV. Summary of the obtained results and possible improvements are then discussed in the conclusion.

II. NUMERICAL METHODS

A. Wave propagation in turbulent medium

For a wave field $\Phi=\psi(y,z)e^{-i\kappa x}$ propagating in x direction, the amplitude ψ satisfies the parabolic approximation to the wave equation [24]

$$2i\kappa\frac{\partial\psi}{\partial x}+\nabla_\perp^2\psi+2\kappa^2 n'\psi=0, \tag{1}$$

where $\kappa=2\pi/\lambda$ is the wave number; $n'=n-\langle n\rangle$ is the fluctuating part of refractive index and $\nabla_\perp^2$ is the Laplacian. $\langle\ \rangle$ denotes spatial averaging. Equation (1) can be solved numerically using the Fourier split-step methods for its accuracy and speed [25]. The split-step solution of ψ at $x+\Delta x$ is given as:

$$\psi(x+\Delta x,y,z)=e^{i\phi}F^{-1}[\psi(x,K_\perp)e^{-iK_\perp^2\Delta x/(2\kappa)}] \tag{2}$$

where, F^{-1} indicates the two-dimensional (2D) inverse Fourier transform in the plane perpendicular the propagation direction (transverse plane) and $\psi(x,K)$ is the Fourier transform of ψ at x. $K_\perp=(k_y^2+k_z^2)^{1/2}$ is the wave number in the transverse plane. The phase ϕ in Eq. (2) is related to the refractive index fluctuations n' of the medium through Eq. (3)

$$\phi(x,y,z)=\kappa\int_x^{x+\Delta x}n'(x,y,z)dx. \tag{3}$$

As the wave propagates through the medium, divided into thin slabs of thickness Δx, each slab introduces random contribution to the wave phase, but essentially no change in the amplitude. Amplitude variations build up by diffraction over many slabs. It is for this reason these slabs are also known as phase screens and the method multiple phase-screen method. The details of the method can be found in [9]. This method is based on the Markov's approximation [26,27], according to which a continuous random medium can be decomposed into a series of statistically independent phase screens. This approximation relates 2D phase spectrum $\hat{\phi}$ of each screen with three-dimensional (3D) refractive index spectrum $\hat{n}$ through

$$\hat{\phi}(k_y,k_z) = 2\pi\kappa^2\Delta x\hat{n}(k_x=0,k_y,k_z). \quad (4)$$

The phase is then generated using the following discrete version of 2D inverse Fourier transform:

$$\phi(j\Delta y,l\Delta z) = \sum_{n=0}^{N_y}\sum_{m=0}^{N_z}[a(n,m)+ib(n,m)] \times\exp[2\pi i(jn/N_y+lm/N_z)] \quad (5)$$

where, $i^2=-1$; Δy and Δz are the grid spacing in the phase screen; N_y and N_z are number of points in the respective directions; and $a(n,m)$ and $b(n,m)$ are the zero mean Gaussian uncorrelated random numbers with

$$\langle a^2(n,m)\rangle = \langle b^2(n,m)\rangle = \Delta k_y\Delta k_z\hat{\phi}(n\Delta k_y,m\Delta k_z). \quad (6)$$

Here, $\langle\ \rangle$ denotes ensemble average and $\Delta k_y=2\pi/(N_y\Delta y)$ and $\Delta k_z=2\pi/(N_z\Delta z)$ are the grid size of k_y and k_z in the spectral plane. The phase spectrum $\hat{\phi}$ is obtained from Eq. (4) using a suitable refractive index spectrum. For the present study, we have used the modified von Karman spectra of [18] to represent a realistic atmospheric boundary layer. This modified spectrum includes the effect of outer scale L_0, through the basic von Karman spectrum and the effect of inner scale l_0 through the realistic dissipation range model of [28]. It is given by

$$\hat{n}(K) = 0.0330054C_n^2(K^2+1/L_0^2)^{-11/6}f[Kl_0] \quad (7)$$

where, $K=(k_x^2+k_y^2+k_z^2)^{1/2}$ is the magnitude of the three-dimensional wave vector; $f(x)=(1.0+0.70937x+2.8235x^2-0.28086x^3+0.08277x^4)e^{-1.109x}$ shows the effect of the inner scale in the dissipation range [28]; C_n^2 is the refractive index structure function parameter which determines the strength of turbulence in the medium. A schematic of refractive index spectrum, showing relevant length scales of turbulence, is displayed in Fig. 1 for better understanding.

It is to be noted that the algorithm described above does not include the effect of scales larger than the screen size. Therefore, ideally, in order to include the size of the scales of the order of L_0, the screen size should be sufficiently larger than L_0. For real atmospheric turbulence, in which L_0 ranges from few meters to few hundreds of meters, achieving this task is known to be very computationally expensive [29]. An efficient technique was proposed in [29] to account for the effects of large scale phase fluctuations. This technique has been used in many previous works, including that of [11], in which the accuracy of the technique was validated against the simple fast Fourier transform (FFT) based method. We have adopted the same algorithm in the present work, which involves addition of extra phase term, ϕ_{SH}, to the main phase term in Eq. (5). This extra phase term is given as [11]:

$$\phi_{SH}(j\Delta y,l\Delta z) = \sum_{p=1}^{N_p}\sum_{n=-1}^{1}\sum_{m=-1}^{1}[a(n,m,p) + ib(n,m,p)]\exp[i(2\pi/3^p)(jn/N_y+lm/N_z)] \quad (8)$$

with,

$$\langle a^2(n,m,p)\rangle = \langle b^2(n,m,p)\rangle = \frac{\Delta k_y}{3^p}\frac{\Delta k_z}{3^p}\hat{\phi}(n\Delta k_y/3^p,m\Delta k_z/3^p), \quad (9)$$

if $n\neq 0$ and $m\neq 0$. Here, $\Delta k_y/3^p$ and $\Delta k_z/3^p$ are the spectral domain grid sizes for subharmonic of order p. These subharmonics are added to replace the origin in the Fourier space. The order of the subharmonic, p, determines the largest allowable scale in the simulation, i.e., $p=2$ implies an outer scale of turbulence 3^2 times larger than the size of the phase screen. In the present simulation, the value of p is determined to include the effect of scales as large as $3L_0$. Therefore, for a phase screen of size 1 m $\times$ 1 m and $L_0\sim 71$ m, we need to include $p=5$ subharmonic set to include the effect of scales as large as $3L_0$.

The required number of phase screens depend on the propagation distance and C_n^2. For the simulations in the present work, 40 screens are used for a propagation distance of 6 km. The number of points, $N_y\times N_z$, for each phase screen should be chosen correctly to include the effect of scales of the order of inner scale of turbulence. This is necessary to get correct information of the small scale phase fluctuations [30]. For the present work, $N_y=N_z=512$ is used for wave of wavelength $(\lambda)=0.6$ μm and screen size 1 m, so that the grid size is much smaller than the inner scale value ($\sim$0.02 m) used in the present simulation. The rationale for taking screen of size 1 m $\times$ 1 m is explained below.

B. Vortex tracking algorithm

Optical vortex is designed using the standard LG beams that is written at the source plane (x=0) as:

$$\psi_{p,q}(r,\theta,x=0) = A_{p,q}\left(\frac{\sqrt{2}r}{w_0}\right)L_q^{(p)}\left(\frac{2r^2}{w_0^2}\right)\exp[ip\theta - r^2/w_0^2], \quad (10)$$

where $r=\sqrt{(y-y_0)^2+(z-z_0)^2}$ is the radius and $\theta=\tan^{-1}(\frac{y-y_0}{z-z_0})$ is the angular location of a point in the source plane, (y_0,z_0) represents the center of the beam, w_0 is the width of the beam in the source plane, $L_q^{(p)}$ are the associated Laguerre functions, and A_{pq} is a normalization constant. Here, the integer q represents the radial order of the beam and p represents the azimuthal order or the charge of the beam. For the present study, we have used a beam with $p=\pm 1$ and $q=0$ for its simplicity in tracking the path of the primary vortex. The initial beam width is taken as $w_0=0.02$ m and the phase-screen size is $50w_0$ (=1 m). Screen size is chosen so that the signal amplitude ($|\psi_{1,0}(r,\theta)|$), at any x, is negligibly small near the boundaries. This is necessary to avoid the effect of aliasing due to the inherent periodicity involved with the phase-screen method [30].

The vortex tracking technique used in the present work is based on the contour tracing algorithm. For a phase screen, at a certain distance from the initial one, the implementation of the vortex tracking algorithm is detailed below in a step-by-step manner:

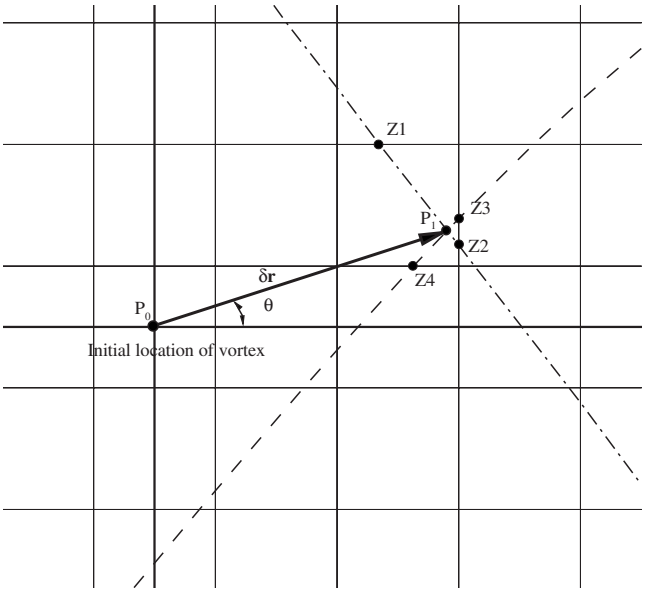

FIG. 2. A schematic diagram explaining the vortex search algorithm. The thin solid lines are the grid cells within the search area A_0. The dashed and the dash-dotted lines are the zero contours of Re(ψ) and Im(ψ), respectively, and the zeros due to them ($Z1$, $Z2$, $Z3$, and $Z4$) are shown as black dots in the diagram. The thick solid lines are the axes system, the center of which correspond to the initial location of the vortex (P_0). The point P_1 correspond to location of the vortex after traveling through the turbulent atmosphere.

(i) Define an area, A_0, on the current phase screen in order to search for the vortex. In the present case we have used a square of size $A_0 = w_0 \times w_0$.

(ii) On each grid cell, within A_0, find the number of zeros due to the real [Re(ψ)] and the imaginary part [Im(ψ)] of ψ. Because the values ψ is already known at each vertex of the cell (solution of Eq. (2)), zeros can be easily calculated by using any standard interpolation algorithm. In the present case linear interpolation is used.

(iii) Locate the cell(s) with two zeros due to Re(ψ) and two zeros due Im(ψ). It is to be noted that a grid cell, with four mutually perpendicular sides, can only have a maximum of two zeros of a given function. One such cell is shown in the schematic of Fig. 2, with the zeros $Z1, Z2$ due to Im(ψ), and zeros $Z3, Z4$ due to Re(ψ).

(iv) Join the two zeros to form the zero contour line corresponding to Re(ψ) and Im(ψ). In the present case the two zeros have been joined using a straight line. The dashed line in Fig. 2 is the contour line of Re(ψ)=0 and the dash-dotted line is the contour line of Im(ψ)=0.

(v) The point of intersection of these two lines, one from Re(ψ)=0 and another from Im(ψ)=0, give the location of the vortex in that cell. Note the vortex P_1 in Fig. 2.

The algorithm is explained graphically in Fig. 2, where the zero contour line corresponding to Re(ψ) and Im(ψ) are shown as dashed and dash-dotted lines, respectively. The grid cells inside A_0 are shown as square boxes. The initial location of the vortex (as projected onto the current phase screen) is marked as point P_0 and its current location is marked as point P_1 in the figure.

The location and the number of vortices as obtained using the algorithm are stored for its later use. In case no vortex is found in A_0, the area is increased by a small amount unless, at least, one vortex is found. It is to be noted that for our present use, we need to track the primary vortex without getting confused by any secondary vortex, formed during the propagation. We have observed from our simulations that if the screen size is sufficiently large, it is very rare to have some secondary vortex come into the area of search discussed above. In case it does, it is advisable to chose the vortex closest to the primary vortex in the previous plane. Of course, in such cases, it is always better to keep smaller step size (Δx) to ensure that the same vortex is being followed.

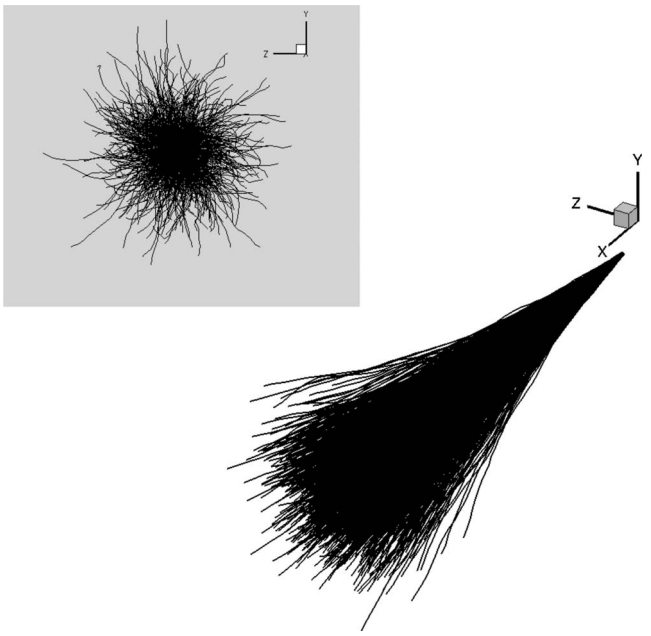

FIG. 3. Different trajectories of the vortex from 1000 different realizations of random numbers.

III. VORTEX TRAJECTORY

By the word, *vortex trajectory*, we mean the locus of the phase singularity, of the initial beam, $\psi_{p,q}(x=0)$, as tracked using the algorithm detailed above. Obviously, this job is relevant only when $p>0$ (for any value of q), because then it is possible to trace a curve corresponding to the trajectory of the phase singularity, which can be precisely defined as point of intersection Re(ψ)=Im(ψ)=0. As already mentioned, we have used a beam with $p=\pm 1$ and $q=0$ for its simplicity in tracking the path of the primary vortex.

The trajectories of the vortex for 1000 different realizations of turbulence are shown in Fig. 3, for some representative value of C_n^2 in an isotropic turbulent medium. It is very clear from the figure that different realizations start with $z=y=0$, and then it keeps on increasing with propagation distance. The figure in the inset shows the transverse projection of the trajectories (as seen standing at the end of the propagation path). This figure shows that trajectories are scattered in all the directions, in a uniform manner, forming a circular patch at any transverse plane in the propagation path. Also, the curves due to each realizations vary smoothly in the

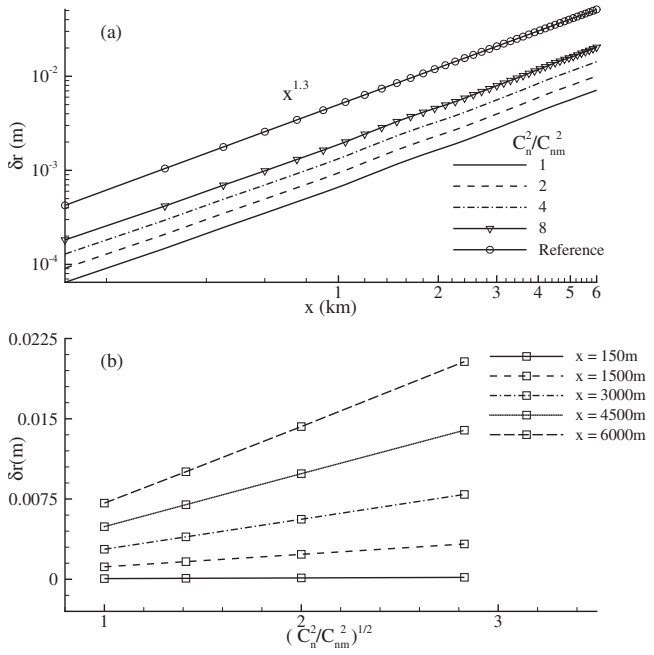

FIG. 4. (a) Variation in radial departure (δr), with propagation distance (x) (log-log scale), at the indicated values of C_n^2/C_{nm}^2. Its functional dependence on x, following Eq. (12), is also shown as a reference line proportional to $x^{1.3}$ (b) Variation in δr with $\sqrt{C_n^2/C_{nm}^2}$ is shown at indicated values of x.

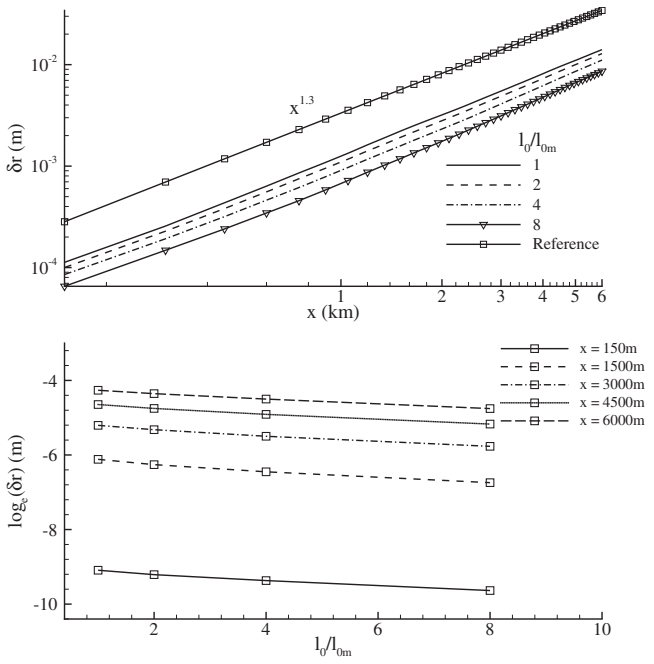

FIG. 5. (a) Variation in radial departure (δr), with propagation distance (x) (log-log scale), at the indicated values of l_0/l_{0m}. Its functional dependence on x, following Eq. (13), is also shown as a reference line proportional to $x^{1.3}$ (b) Variation in δr with l_0/l_{0m} is shown at indicated values of x.

propagation direction. These findings indicate some kind of existing pattern in the radial departure of the vortex, which is to be explored in the following work.

A. Radial departure

For a vortex located at a point $P_1=(x_1,y_1,z_1)$, its radial departure δr is evaluated as (see Fig. 2):

$$\delta r(x=x_1)=\sqrt{(y_1-y_0)^2+(z_1-z_0)^2} \tag{11}$$

where, $P_0=(x_0,y_0,z_0)$ is the initial location of the vortex. In order to get statistically converged behavior in δr, its final value needs to be obtained after averaging over different realizations of random numbers.

For the case of isotropic turbulence, the variation in δr, with the propagation distance x, for different turbulent intensities (C_n^2), for constant value of $L_0=71$ m and $l_0=0.0176$ m is shown in Fig. 4(a). Note that the turbulent intensities have been nondimensionalized in the figure with the lowest value of $C_n^2=C_{nm}^2=0.716\times10^{-16}$ $m^{-2/3}$. These results are obtained after averaging over 100 different realizations. It was found that 100 realizations are optimum to get a statistically converged result on δr. The shown result clearly indicate the linear dependence of δr on x (in log-log scale), which can be formulated as:

$$\delta r=x^m F(C_n^2,L_0,l_0,w_0,\kappa)\quad (x>0). \tag{12}$$

Here, $m\approx1.3$ is the slope of the lines (obtained numerically) in Fig. 4, whose exact value will be evaluated later, based on dimensional analysis. F in Eq. (12) above indicates the functional dependence of δr on turbulent parameters (C_n^2,L_0,l_0), wavelength $(2\pi/\kappa)$ and the beamwidth (w_0). As already mentioned in the introduction, our interest in the present work is to find a relationship between the vortex trajectory and the turbulent parameters. Therefore, the dependence on other parameters have been ignored in the future discussions. It is important to note that δr keeps on increasing with x and in order to have it unaffected by the boundary condition, the screen size must be chosen sufficiently large.

The variation in δr with $\sqrt{C_n^2/C_{nm}^2}$ is shown in Fig. 4(b) for different values of x in Fig. 4(a). From the figure we can conclude that at a given x, for constant L_0 and l_0, δr is linearly dependent on $\sqrt{C_n^2}$. Applying this conclusion on Eq. (12), keeping in mind that $\delta r=0$ for $C_n^2=0$, gives us

$$\delta r=x^m\sqrt{C_n^2}F(L_0,l_0)\quad (x>0). \tag{13}$$

A proportionality constant is left to include in the equation above, which we will include later, after including the effects of l_0 and L_0. Next we show the variation in δr, with x, for different values of l_0/l_{0m} in Fig. 5(a). Here, $l_{0m}=0.0176$ m correspond to the lowest value of l_0 used in the figure. These plots are obtained for a constant value of $C_n^2=2.865\times10^{-16}$ $m^{-2/3}$ and $L_0=71$ m. This figure, confirming the $x^{1.3}$ dependence of δr on x, shows that the radial departure of the vortex decreases with increasing l_0. In order to understand the effect of l_0 more precisely, variation in $\log_e(\delta r)$ with l_0/l_{0m} is shown in Fig. 5(b), for different values of x in Fig. 5(a). From Fig. 5(b) we can conclude that at a given x, for constant L_0 and C_n^2, $\log_e(\delta r)$ is linearly dependent on l_0. Applying this conclusion on Eq. (13) gives us

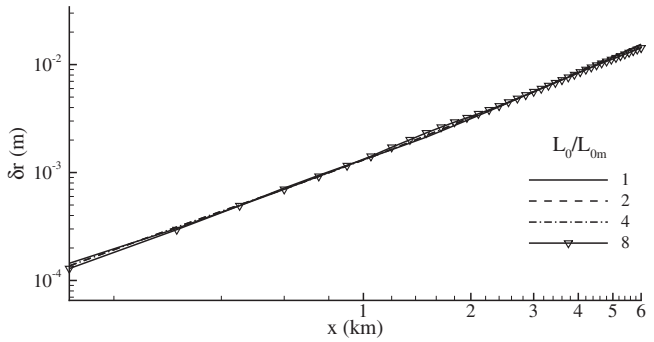

FIG. 6. Variation in radial departure (δr) with propagation distance (x) (log-log scale) at the indicated values of L_0/L_{0m}. Note: $L_{0m}=8.875$ m.

$$\delta r = x^m \sqrt{C_n^2} e^{a l_0} F(L_0) \quad (x > 0). \tag{14}$$

Value of a in then calculated numerically as the slope of the curves in Fig. 5(b). Using a second-order scheme to calculate the derivative, we get $a=-2.1\pm0.3$.

Effect of L_0 on δr was found very weak even for large variation in the values of L_0. This can be verified from the Fig. 6, which shows the variation in δr with x for different value of L_0/L_{0m}. Here, $L_{0m}=8.875m$ for which the value p (see Eq. (8)) was taken to be equal to 3.

Therefore, in the final form, the equation describing the dependence of δr on C_n^2, L_0, and l_0, reduces from Eq. (14) to

$$\delta r = A x^m \sqrt{C_n^2} e^{a l_0} (x > 0), \tag{15}$$

for A being a unit-less proportionality constant. In order to check the dimensional correctness of the equation above, we performed dimensional analysis of the Eq. (15), and found that $m=4/3$. This value is very close to the value, $m=1.3$, obtained from the slope of the lines in Fig. 4. This match in the values of m, as obtained from two different methods, provides a check on the validity of Eq. (15). The value of A can be obtained from any reference result. From our collection of the results, using $a=-2.1$ and $m=4/3$, we found $A=7.62\pm0.6$ confirms the expression of Eq. (15) in all of the cases.

It is important to realize that the observed effect of the inner scale, clearly justifies the use of modified spectrum, Eq. (7), in the propagation study of optical vortices. Equation (15) also suggests that an optical vortex suffers less distortion, while propagating through a turbulent media with larger value of l_0, than a similar media with smaller l_0. This can also be seen in Fig. 5. Effect of higher values of C_n^2, as expected, is to cause more distortion to the propagating vortex. Furthermore, our results also indicate that the turbulent scales (K^{-1}) of the order of

$$\frac{K^{-1}}{w_0} > \frac{L_{0m}}{w_0} = 443.75, \tag{16}$$

do not play significant role in deciding the propagation characteristics of optical vortices.

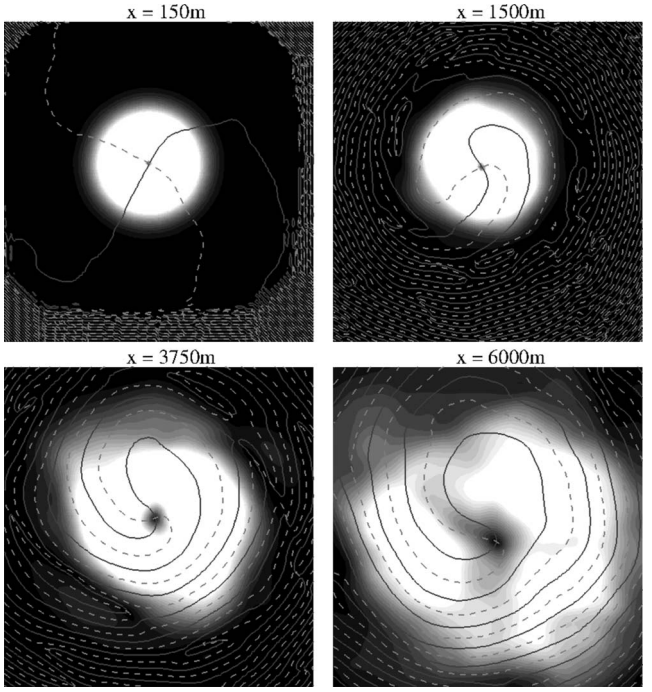

FIG. 7. Wave intensity contours (close-up view) of isotropic case. The vortex location is marked as the point of intersection of the solid ($\mathrm{Re}(\psi)=0$) and the dashed ($\mathrm{Im}(\psi)=0$) lines.

Eq. (15) could be useful for researchers working in atmospheric turbulence, and in optical wave propagation, as it can be used to investigate the effect of turbulence on the propagation properties of optical vortices and vice versa. Equation (15) provides a direct relationship between the propagation property of the optical vortex and the properties of turbulence. It can be used to estimate the structure function parameter and the inner scale of any turbulent medium using the information on the radial departure (δr) of the optical vortex. This provides the first step to solve the inverse problem. Note that this approach is quite different from previous studies [2,15,17] about interaction between optical vortex and turbulence. In the current approach, the interaction is not only studied to know the impact on the properties of the optical vortex but also to investigate, more deeply, the relevant parameters of turbulence.

B. Angular orientation

The results obtained above correspond to the case of homogeneous and isotropic turbulence. Anisotropic effects in this synthetic scalar turbulent field can be generated, in a very simple manner, by changing the definition of K in Eq. (7) to:

$$K = (c_x k_x^2 + c_y k_y^2 + c_z k_z^2)^{1/2} \tag{17}$$

where, c_x, c_y, and c_z are the respective wave coefficients. In order to see the effect of anisotropy on the propagation of an optical vortex wave intensity contours are shown for an isotropic case ($c_x=0$, $c_y=1$, and $c_z=1$) and an anisotropic case ($c_x=0$, $c_y=3$, and $c_z=1$) in Figs. 7 and 8, respectively. The contours show the close-up view of the field, at different

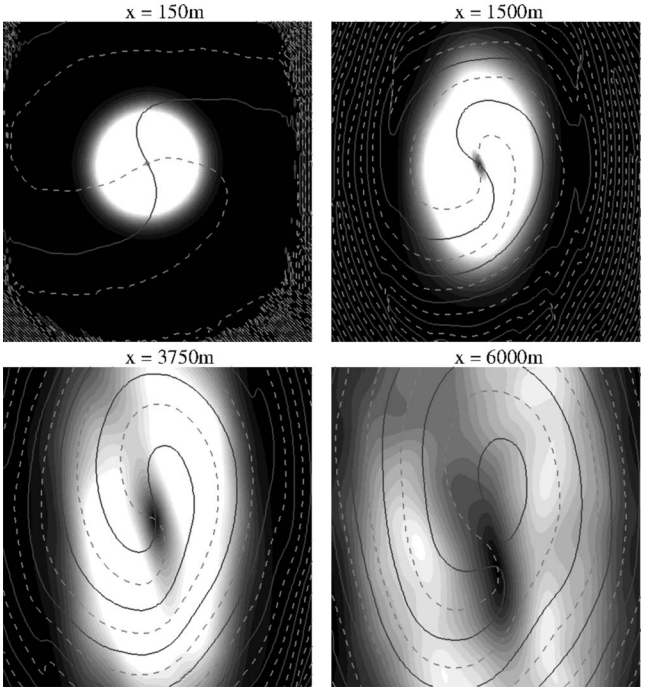

FIG. 8. Same as Fig. 7 except for anisotropic case.

locations in the propagation direction, for typical values of the turbulent parameters ($C_n^2=2.865\times10^{-16}$ m$^{-2/3}$, $l_0=0.0176$ m, and $L_0=71$ m). The vortex location is marked in the figure as the point of intersection of the solid $[\mathrm{Re}(\psi)=0]$ and the dashed $[\mathrm{Im}(\psi)=0]$ lines. The stretching effect of turbulent anisotropy is clearly visible in the figure. It is not difficult to make out that the observed stretching in the Y direction is due to the higher value of c_y. In order to further investigate on its effect on δr, three systematic cases using $c_x=0$, $c_y=2$, 3, 4, and $c_z=1$ were run. Comparison of these anisotropy simulation results with those from isotropic case did not show any significant effect of medium anisotropy on δr. Major differences were noted in the angular orientation of the vortex location that is discussed next in greater detail.

The angular orientation of the vortex along with its radial departure gives complete information about its trajectory in a turbulent medium. Angular orientation is defined as the angular departure of the vortex location from the horizontal (+Z axis in the present case) and is calculated as (see Fig. 2)

$$\theta=\tan^{-1}\left(\frac{y_1-y_0}{z_1-z_0}\right). \tag{18}$$

From the Fig. 8, one would expect the angular orientation of the vortex to be related to the coefficients c_y and c_z. In order to understand this relation more closely, histogram of θ is obtained from 75 000 different realizations, for the cases: $c_x=0$, $c_y=1$, 2, 3, 4, and $c_z=1$.

Histogram is plotted for number of realizations versus angle of orientation of the vortex, and is shown in Fig. 9 for the cases mentioned above. Angular orientation is measured in the range $[-\pi,+\pi]$, divided equally into 360 parts of size 1° each. The figure indicates the probability of a vortex to be found at a given angle. For the isotropic case ($c_y=1$, $c_z=1$), all the angles show the equal probability, which is in accordance with the results in Fig. 3. As the coefficient c_y is increased from 1 to 2, the isotropy is lost and the vortex shows an orientation preference along the Y direction. This is evident from the development of Gaussian-like peaks at $\theta\approx\pm\pi/2$. As the medium anisotropy is further increased (by increasing c_y to 3 and 4), the probability of the vortex to orient themselves along Y direction also increases. This is evident from the decreasing width (hence increasing height) of the Gaussian in Fig. 9.

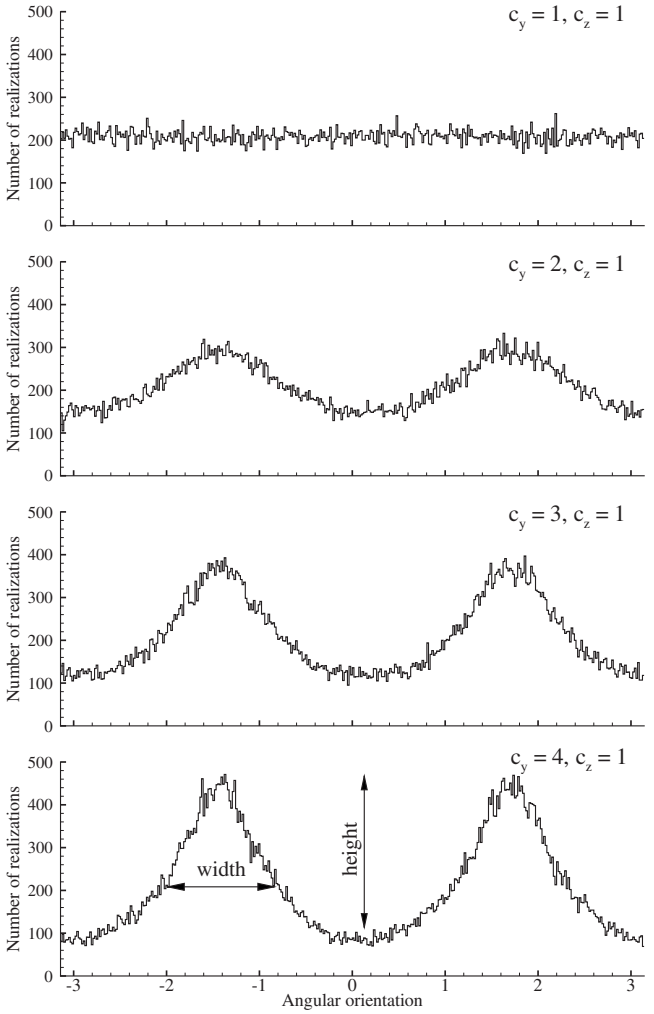

FIG. 9. Effect of anisotropy is shown using histogram for number of realizations versus angular orientation of the vortex. Total number of realizations used is 75 000. Note the width and the height of the Gaussian marked in the last frame.

Although the shown figures correspond to angular orientation of the vortex at x=6 km; the vortex immediately adopts to the anisotropy of the medium, even at distance of the order of 100 m. The important features to note in these plots are:

(i) There is no preferred direction for the vortex in an isotropic medium.

(ii) The preferred direction for $c_y/c_z>1$ is $\pm\pi/2$.

(iii) The width of the Gaussian reduces (hence its height increases) for increase in c_y/c_z.

The features noted above can be interpreted in the similar way for the cases with $c_z/c_y > 1$. For this case (results not shown), the preferred directions are 0 and π.

It is to be noted that the results discussed so far correspond to a vortex of charge=+1. In order to see the effect of polarity, the same simulations were run for charge=−1 and it was noted that the obtained results (not shown) did not show any effect of polarity on the results obtained above.

IV. DRIFT OF OPTICAL VORTEX VS DRIFT OF GAUSSIAN BEAM CENTROID

Transverse drift of the centroid of a simple Gaussian beam has been studied by many authors to understand the turbulence-induced beam spread [31–36]. For some specific cases, analytical expressions are known, a summary of which can be found in [35,36]. To fully realize the importance of the vortex trajectory obtained above, it will be interesting to see how does the drift of an optical vortex compares with the drift of the its parent Gaussian beam centroid. Unfortunately, there are no analytical expressions for the case we are studying. Therefore, in the following we have computed the drift using numerical simulation.

Gaussian beam can be generated by using $p=0$, $q=0$ in Eq. (10). The radius vector of the beam centroid, $\boldsymbol{r_c}$, from the beam geometrical center is defined as [31]

$$\boldsymbol{r_c}(x) = \frac{\int\int \boldsymbol{r} I(x,\boldsymbol{r}) d^2 r}{\int\int I(x,\boldsymbol{r}) d^2 r} \tag{19}$$

where $I(x,\boldsymbol{r})$ is the intensity of the point $\boldsymbol{r}$ on the phase screen at x, and the integration is carried out over the phase screen. Simulation is performed for $C_n^2 = 0.716 \times 10^{-16}$ $\mathrm{m}^{-2/3}$, $L_0 = 71$ m, and $l_0 = 0.0176$ m. These values correspond to the results shown in Fig. 4. The values of r_c thus obtained is subtracted from the already calculated values of δr (from Fig. 4), and their modulus, $|\delta r - r_c|$, is shown in Fig. 10.

Figure clearly shows large differences between the two drifts, both for small as well as large values of x. In between, the difference is less. This implies, keeping in mind that the optical vortex varies as $x^{4/3}$ (see Eq. (15)) throughout its propagation path that the Gaussian beam centroid changes its slope in between. Also, the differences increase proportionally with the increase in C_n^2, indicating a similar dependency of r_c on C_n^2.

V. CONCLUSION

Trajectory of an optical vortex in realistic atmospheric turbulence is studied in this paper using numerical simulations. The trajectory has been identified using the radial departure (δr) and the angular orientation (θ) of the vortex with respect to its initial location. An efficient algorithm is proposed to search for the vortex core. The main result of the paper is to categorize the dependency of δr and θ, on turbulent parameters like C_n^2, l_0, L_0, and anisotropy, respectively. The obtained results can be summarized as:

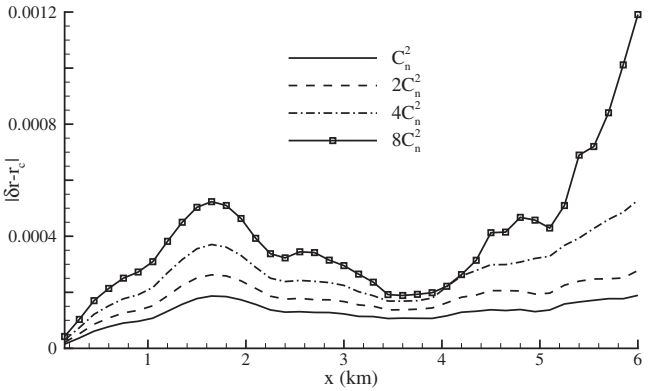

FIG. 10. Difference between the drift (or radial departure) of the optical vortex and the drift of the parent Gaussian beam centroid calculated using Eq. (19).

(a) The radial departure of the vortex is related to C_n^2 and l_0 of the medium through Eq. (15).

(b) The radial departure of the vortex is significantly different from the drift of its parent (Gaussian) beam centroid, specially for higher values of C_n^2.

(c) The angular orientation of the vortex is related to the anisotropy of the medium. This is shown qualitatively through Fig. 9.

(d) Medium anisotropy has negligible effect on δr.

(e) There is no effect of polarity of the vortex on the results obtained in this paper.

The presented work establishes the importance of using a realistic spectrum, for refractive index fluctuations, in the propagation study of optical vortices. Additionally, the present work provides the first step to study the inverse problem, i.e., to investigate the various properties of atmospheric turbulence using the information about the properties of the optical vortex.

The results inferred from the Figs. 5 and 6, are based on a small range of inner and outer scale values. It covers the nondimensional inner scale in the range, $0.88 \leq l_0/w_0 \leq 7.04$, and nondimensional outer scale in the range, $443.75 \leq L_0/w_0 \leq 3550$. It is not possible to comment on the behavior of δr for values outside this range, unless more exhaustive simulations are performed, covering the entire range of these scales. Also, the dependence of angular orientation on medium anisotropy is only qualitatively discussed in the present work. In order to develop some kind of quantitative relationship more simulations with even more number of realizations are required. We plan pursue both these aspects in the due course of time.

[1] J. F. Nye and M. V. Berry, Proc. R. Soc. Lond. A **336**, 165 (1974).
[2] C. Paterson, Phys. Rev. Lett. **94**, 153901 (2005).
[3] N. B. Simpson, K. Dholakia, L. Allen, and M. J. Padgett, Opt. Lett. **22**, 52 (1997).
[4] L. Allen, S. M. Barnett, and M. J. Padgett, *Optical Angular Momentum* (IOP Publishing, Bristol, 2003).
[5] W. M. Lee, X. C. Yuan, and W. C. Cheong, Opt. Lett. **29**, 1796 (2004).
[6] A. Vinçotte and L. Bergé, Phys. Rev. Lett. **95**, 193901 (2005).
[7] Z. Bouchal, Opt. Commun. **210**, 155 (2002).
[8] M. V. Vasnetsov, I. G. Marienko, and M. S. Soskin, JETP Lett. **71**, 130 (2000).
[9] J. M. Martin and S. M. Flatte, Appl. Opt. **27**, 2111 (1988).
[10] W. A. Coles, J. P. Filice, R. G. Frehlich, and M. Yadlowsky, Appl. Opt. **34**, 2089 (1995).
[11] R. Frehlich, Appl. Opt. **39**, 393 (2000).
[12] A. E. Barrios, IEEE Trans. Antennas Propag. **42**, 90 (1994).
[13] G. D. Dockery, IEEE Trans. Antennas Propag. **36**, 1464 (1988).
[14] S. W. Marcus, IEEE Trans. Antennas Propag. **40**, 1451 (1992).
[15] G. Gbur and R. K. Tyson, J. Opt. Soc. Am. A Opt. Image Sci. Vis. **25**, 225 (2008).
[16] K. Zhu, G. Zhou, X. Li, X. Zheng, and H. Tang, Opt. Express **16**, 21315 (2008).
[17] L. G. Wang and W. W. Zheng, J. Opt. A, Pure Appl. Opt. **11**, 065703 (2009).
[18] A. Dipankar and P. Sagaut, J. Atmos. Sci. (to be published).
[19] I. Freund, Opt. Commun. **181**, 19 (2000).
[20] I. Freund and D. A. Kessler, Opt. Commun. **187**, 71 (2001).
[21] R. P. Singh and S. R. Chowdhury, Opt. Commun. **215**, 231 (2003).
[22] M. Chen, F. S. Roux, and J. C. Olivier, J. Opt. Soc. Am. A Opt. Image Sci. Vis. **24**, 1994 (2007).
[23] Regis Marchiano and Jean-Louis Thomas, Phys. Rev. E **71**, 066616 (2005).
[24] A. N. Monin and A. M. Yaglom, *Statistical Fluid Mechanics II* (MIT Press, Cambridge, 1971).
[25] J. R. Kuttler and G. D. Dockery, Radio Sci. **26**, 381 (1991).
[26] A. Ishimaru, *Wave Propagation and Scattering in Random Media* (Oxford University Press, Oxford, 1997).
[27] V. I. Tatarski, *Wave Propagation in a Turbulent Medium* (Translated from the Russian by R. A. Silverman) (Dover, New York, 1967).
[28] R. J. Hill, J. Fluid Mech. **88**, 541 (1978).
[29] R. G. Lane, A. Glindemann, and J. C. Dainty, Waves Random Media **2**, 209 (1992).
[30] D. L. Knepp, Proc. IEEE **71**, 722 (1983).
[31] V. Klyatskin and A. Kon, Radiophys. Quantum Electron. **15**, 1056 (1972).
[32] T. Chiba, Appl. Opt. **10**, 2456 (1971).
[33] H. Yura, J. Opt. Soc. Am. **63**, 567 (1973).
[34] J. Dowling and P. Livingston, J. Opt. Soc. Am. **63**, 846 (1973).
[35] R. L. Fante, Proc. IEEE **63**, 1669 (1975).
[36] R. L. Fante, Proc. IEEE **68**, 1424 (1980).